Article

Effect of Anisotropic Structural Depth on Orientation and Differentiation Behavior of Skeletal Muscle Cells

Jianfeng Chen, Xuefei Chen, Yihao Ma, Yiran Liu, Jin Li, Kai Peng, Yichuan Dai, and Xiaoxiao Chen*

Read Online

ACCESS | Metrics & More | Article Recommendations

ABSTRACT: Extensive research has been conducted to examine how substrate topological factors are involved in modulating the cell behavior. Among numerous topological factors, the vital influence of the touchable depth of substrates on cell behaviors has already been extensively characterized, but the response of cells to the topological structure at untouchable depth is still elusive. Herein, the influences of substrate depth on myoblast behaviors are systematically investigated using substrates with depths ranging from touchable depth (microgrooved) to untouchable depth (microbridges). The results show that an increase in microgroove depth is accompanied by an inhibited cell spreading, an enhanced elongation, and a more obvious orientation along microgrooves. Interestingly, myoblasts located on microbridges show a more pronounced elongation with increasing culture time but a position-dependent orientation. Myoblasts on the center and parallel boundary of microbridges orient along the bridges, while myoblasts on the vertical boundary align perpendicular to the microbridges. Moreover, the differentiation results of the myoblasts indicate that the differentiated myotubes can maintain this position-dependent orientation. The simulation of the stress field in cell monolayers suggests that the position-dependent orientation is caused by the comprehensive response of myoblasts to the substrate discontinuity and substrate depth. These findings provide valuable insights into the mechanism of cell depth sensing and could inform the design of tissue engineering scaffolds for skeletal muscle and biohybrid actuation.
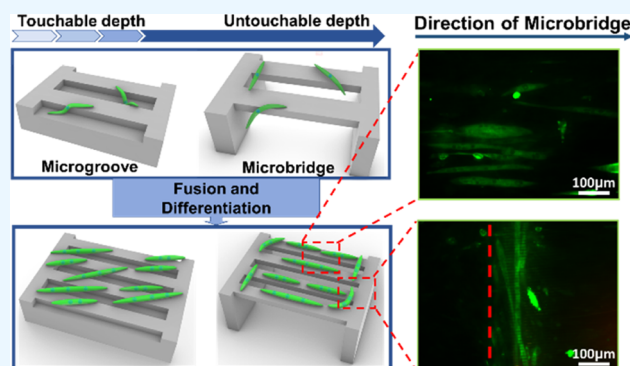
1. INTRODUCTION

Myoblasts are typical anchoring-dependent cells, and their interaction with the microenvironment plays a crucial role in cellular behavior regulation and functional maintenance. Myoblasts are immersed in a complex microenvironment composed of various chemical and physical cues.[1−5] Among these cues, substrate topography has been proven to exert a profound influence on various cell behaviors, including orientation, migration, polarization, adhesion, and so on.[6−8] Many studies have been devoted to exploring the regulatory effects of topological patterns on cell behavior.[6,9−11] For example, micropillar arrays can change substrate stiffness and affect cell elongation and spreading,[12−15] while the shape and size of microwells can determine cell morphology.[16] For muscle tissue regeneration, the uniform orientation of myoblasts plays a crucial role in ensuring the structural and functional integrity of muscle tissue.[17−19] Therefore, to achieve skeletal muscle regeneration in vitro, it is urgent to explore the influence of topological cues on the orientation regulation of myoblasts.

Anisotropic topological patterns (such as oriented microfibers,[20,21] microgrooves,[22] etc.) have been proven to play a vital role in guiding cytoskeletal rearrangements and modulating myoblast orientation and function,[22−24] which is known as contact guidance.[25−27] Rectangular grooves of various sizes are commonly used to investigate contact guidance in vitro and mimic physiological topography (e.g., aligned collagen fibers or tissue clearance) encountered by cells in vivo.[22,28]

Recent research has already demonstrated that the aspect ratio and dimensions of microgrooved substrates exquisitely regulate cellular behaviors and have a vital influence on cell orientation. Human mesenchymal stem cells (hMSCs) exhibit typical orientation along substrates containing grooves with feature sizes ranging from tens to hundreds of microns, and they bridge across grooves when the aspect ratio is less than two.[29] As the critical size of substrates increases from nanoscale to hundreds of micrometers, the response of cells to the grooves becomes weaker and eventually similar to that of the cells on the flat substrate.[10,30−33] Moreover, there is growing evidence that the depth of the topological structure also has a critical influence on cell behaviors.[34] The murine neural progenitor cells (NPCs)
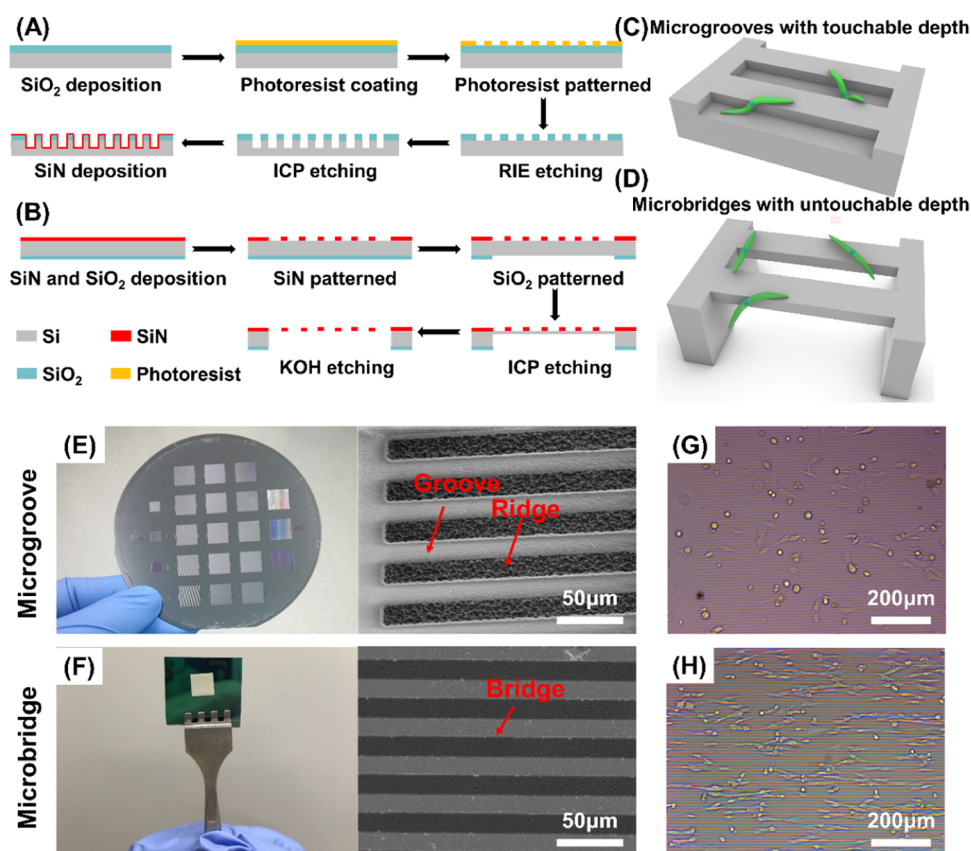
Figure 1. Fabrication process of the microgrooved substrates and microbridge SiN array. (A) Briefly, SiO$_2$ films were deposited on the silicon wafer and patterned by RIE etching after exposure and development of the photoresist layer. After that, the microgrooved substrates were fabricated using ICP and SiN film was deposited to enhance the biocompatibility. (B) SiN and SiO$_2$ films were deposited and patterned as described above. Then, bulk silicon was etched by ICP etching and residual silicon was etched with KOH solution. (C, D) Illustrations of microgrooves with touchable depth and microbridges with untouchable depth. (E, F) Photograph and SEM images of microgroove and SiN microbridge array. White bars equal 50 μm. (G, H) Phase contrast image of microgroove and microbridge substrates seeded with cells. White bars equal 200 μm.

can sense the depth of microgroove substrates and exhibit ordered orientation and enhanced elongation with increasing depth.[35,36] Besides, the depth of microgrooves has been proven to affect cell proliferation and differentiation.[37] Although numerous studies have already extensively characterized the vital influence of the touchable depth of substrates on cell behaviors, the response of cells to an untouchable depth remains elusive. Thus, it is necessary to systematically study the effect of anisotropic topological depth on the orientation of myoblast cells, to reveal the mechanism of cell depth sensing and assist in muscle tissue regeneration.

Herein, a series of microgrooved substrates with touchable depths (0, 0.5, 2 μm) and microbridge substrates with untouchable depth are fabricated to determine the influence of substrate depth on cell behaviors. Then, cell morphology is quantified by measuring the spreading area, aspect ratio, and alignment angle of cells on substrates. Quantitative results show that the inhabited spreading, enhanced elongation, and orientation of myoblasts are caused by the synergistic influence of topology and substrate depth. Moreover, microgrooved substrates result in a bias-angular cell orientation across the entire substrate. Compared with the microgrooved substrates, microbridged substrates have a greater promotion effect on cell elongation. Interestingly, C2C12 cells show a position-dependent orientation on microbridge substrates. Cells on the center or parallel boundary of microbridges display a dominant orientation along the microbridges, while cells on the vertical boundary show a perpendicular orientation to microbridges. The stress field in cell monolayers shows that the cell position-dependent orientation on the microbridge structure is a unique biomechanical behavior that responds to cell depth sensing and substrate discontinuity. The position-dependent orientation makes it possible to achieve heterogeneous cell orientations on a single substrate, revealing its potential application in engineered skeletal muscle patterning for multifunctional bioactuation.

2. EXPERIMENTAL SECTION

2.1. Substrate Fabrication. Microgrooved substrates with lengths and widths of 2000 and 5 μm and different depths (0.5, 2 μm) were fabricated (Figure 1A). First, the silicon dioxide (SiO$_2$, 2 μm) film was deposited on a silicon wafer (400 μm in thickness) using plasma-enhanced chemistry vapor deposition (PECVD). Then, an AZ6112 photoresist with a thickness of 1 μm was spin-coated on the wafer as a mask layer. After being baked at 95 °C for 60 s, lithography with 2 s exposure through contact printing was developed using an ultraviolet aligner (SUSS MA 6). Then, AZ-MIF 400 solution and deionized water were used for the photoresist development and cleaning, respectively. After being baked at 120 °C for 2 min, the SiO$_2$ film was patterned by reactive ion etching (RIE, OXFORD) with 50 sccm CHF$_3$ gas and 5 sccm O$_2$ gas. Using silicon dioxide as a sacrificial layer, the master substrate consisting of microgrooves was created by induction coupling plasma etching (ICP

etching). Finally, the silicon nitride (SiN) layer was deposited to enhance the biocompatibility of substrates.

Microbridge substrates with a length, width, and thickness of 2000, 5, and 0.5 μm, respectively, were fabricated as reported previously (Figure 1B).[38] First, a 0.5 μm-thick SiN film was deposited on a silicon wafer by PECVD. Second, a 2 μm-thick SiO$_2$ layer was deposited by PECVD on the back side of the silicon wafer as an etching barrier layer. The SiN film was patterned as described above. Then, a 10 μm-thick AR-P 3210 positive photoresist was spin-coated on the back side of the SiO$_2$ layer and exposed using a UV aligner for 25 s. After that, the wafer was developed in AR 300−26 solution. The back side of the SiO$_2$ film was also patterned by RIE etching with 25 sccm CHF$_3$ gas and 25 sccm Ar gas. ICP etching was used to etch most of the bulk silicon with a SiO$_2$ layer as the mask. Finally, the residual bulk silicon was etched by KOH solution and microbridges were obtained in a liquid environment.

The final structure of microgrooves and microbridge substrates was determined using a scanning electronic microscope (FE-SEM 8500).

2.2. Cell Culture and Myotube Differentiation. The substrates were first immersed in a phosphate-buffered saline (PBS) solution and sterilized under ultraviolet light for 1 h. C2C12 myoblasts (purchased from Cell Bank of Chinese Academy of Sciences, China) were cultured in Dulbecco's modified Eagle medium (DMEM, Gibco) supplemented with 10% fetal bovine serum and 1% streptomycin/penicillin (Gibco) and incubated at 37 °C and 5% CO$_2$. Cells were lifted with 0.25% Trypsin-EDTA (Gibco) at 37 °C for 30 s and harvested after being centrifuged at 1000 rpm for 5 min. Then, cells were immersed with fresh DMEM and aspirated by gently pipetting to form cell suspensions again. Finally, the cells were resuspended with culture medium to adjust the cell concentration to 1×10^6 cells/mL and incubated for 30 min for cells adhesive to the substrate after seeding.

For myotube differentiation, the substrates seeded with C2C12 cells were placed in a 60 mm Petri dish with growth medium until the cells reached 90% confluence. Then, the growth medium was replaced with differentiation medium (DMEM supplemented with 2% horse serum (Gibco) and 1% penicillin−streptomycin) for myogenic differentiation. The differentiation medium was changed every day to allow for the adequate differentiation of myotubes.

2.3. Immunofluorescence Staining. For myotube immunostaining, the differentiated C2C12 cells were fixed and permeabilized using 4% (w/v) formaldehyde (Invitrogen) for 15 min, washed three times with Dulbecco's phosphate-buffered saline (DPBS, Gibco), and then permeated with 0.5% Triton X-100 solution (Invitrogen) for another 15 min. After being washed with DPBS three times, the myoblasts were blocked with 3% bovine serum albumin (BSA, Invitrogen) at room temperature for 1 h. Then, the substrates with the myotube were immersed in primary mouse monoclonal antibody MY-32 (M1570, Sigma) at a dilution of 1:400 in DPBS and incubated at 4 °C overnight in the dark. On the next day, the substrates were washed with DPBS three times gently, then treated with goat antimouse Alexa Fluor 488 antibody (ab-150113, Abcam, Japan) at a dilution of 1:500 in DPBS, and incubated at room temperature in the dark for 1 h. Then, the stained samples were imaged with fluorescence microscopy (Leica DMI 3000b, Germany).

2.4. Morphology and Alignment. The outline of myoblasts was delineated manually using a brush within Fiji/

ImageJ and fitted with ellipses. Then, the morphology of myoblasts was quantified by analyzing the aspect ratio of myoblasts, which is defined as the ratio of the short axis to the long axis of the ellipse. The cell alignment angle is the angle between the long axis of cell contours and the edge of microgrooves or microbridges. Cells having an alignment angle within $\pm 10°$ are considered to be aligned along microgrooves or microbridges.

The myotube contours were manually outlined using Fiji/imageJ and fitted with an ellipse. The myotube morphology was characterized by the aspect ratio, which refers to the ratio of the long axis and short axis of the ellipse. Alignment angles of myotubes were the angles between the long axis and the edge of microgrooves or microbridges.

2.5. Simulation of Shear Stress and Principle Stress. Commercially available finite element software ANSYS was used to calculate the stress field of a single cell layer on the substrate. Due to the self-contraction of the cytoskeleton, the cell was modeled as an elastic entity with a prestrain of ϵ_0, which results in the deformation of the elastic substrate through adhesion. The experimental results indicated that the prestrain ϵ_0 of the cell is approximately 0.1 under physiological conditions. Consequently, the cell layer was simulated as a 2 μm-thick elastic thin plate. To discretize the cell layer, a layer of solid 186 elements with a mesh size of about 4 μm was employed. The cell achieved self-contractility via thermal strain. Therefore, the thermal expansion coefficient of the cell layer was set as 0.1, which means that a decrease of 1 °C will result in a prestrain of 0.1. Then, the adhesion between the cell layer and the substrate was modeled as a spring with an area stiffness of 0.00125 nN·μm^{-3}, while one side of the cell layer was securely fixed to the rigid substrate surface by using distributed springs.

2.6. Image and Statistical Analysis. All images, captured using a Leica DMI3000B (Leica, Germany) microscope by phase contrast and fluorescent mode, were analyzed with Fiji/ImageJ software.

All data are the mean ± standard deviation (SD) of at least three independent samples per experiment. Statistical significance between experimental groups was analyzed using one-way analysis of variance (ANOVA) followed by Tukey's multiple comparison test with Origin software. Statistical significance is denoted as follows: * $p < 0.05$, ** $p < 0.01$, *** $p < 0.001$. All graphs are drawn using Origin.

3. RESULTS

3.1. Fabrication of the Substrate with Varying Topography. The microgrooved substrates with the same width (5 μm) and touchable depths (2, 0.5 μm) were formed, as depicted in Figure 1A,C. First, SiO$_2$ (2 μm) was etched using RIE etching under the protection of the patterned photoresist layer. Then, the silicon wafer was etched by ICP etching and the silicon nitride layer was deposited to enhance its biocompatibility. The suspended microbridges with a length, width, and thickness of 2000, 5, and 0.5 μm, respectively, were fabricated using the convection freeze sublimation (CFS) method as shown in Figure 1B.[38] First, SiN (0.5 μm) and SiO2 (2 μm) film were deposited. Then, under the protection of the patterned photoresist layer, the silicon nitride film was patterned using RIE. Patterned SiO$_2$ was formed using back-side lithography and RIE. Finally, the residual silicon was removed using ICP etching and KOH wet etching, and microbridges with untouchable depth were formed (Figure 1D).
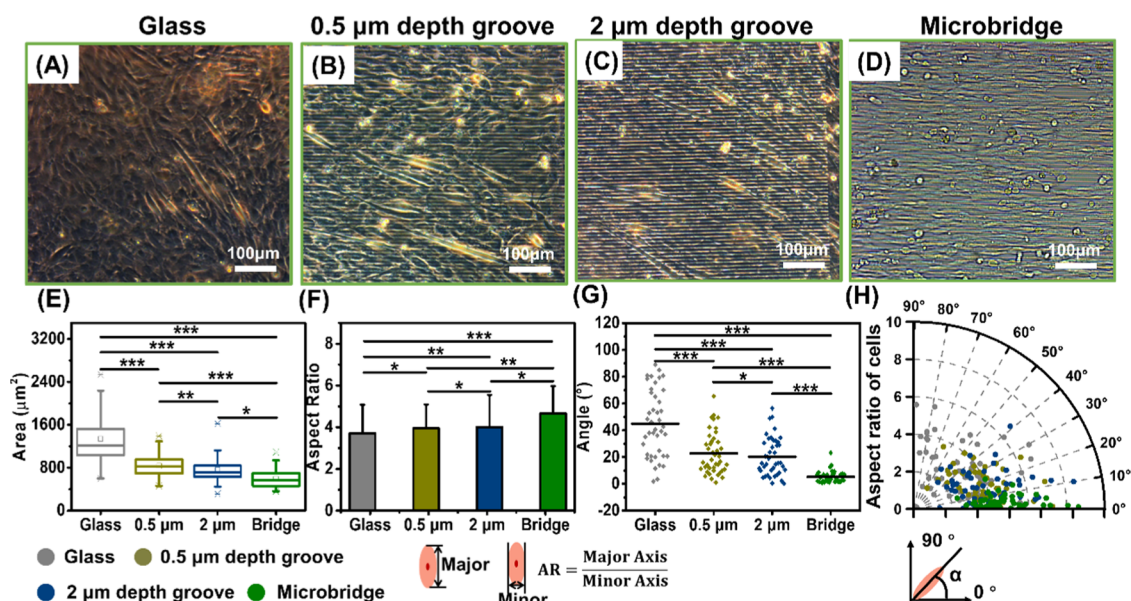
Figure 2. (A–D) Phase contrast images of cells seeded on bare glass, microgrooved substrates (depth of 0.5, 2 μm), and microbridges. (E–G) Area, aspect ratio, and directional distribution of C2C12 myoblast cells cultured on bare glass (gray), 0.5 μm microgrooves (golden), 2 μm microgrooves (blue), and microbridges (green) for 72 h, respectively ($n = 50$). (H) Polar plot of the elongation and orientation of cells on bare glass (gray), 0.5 μm microgrooves (golden), 2 μm microgrooves (blue), and microbridges (green). In the polar plot, AR is the aspect ratio of the cell, and θ (deg) is the angle between the long axis of the cell and the microgroove.
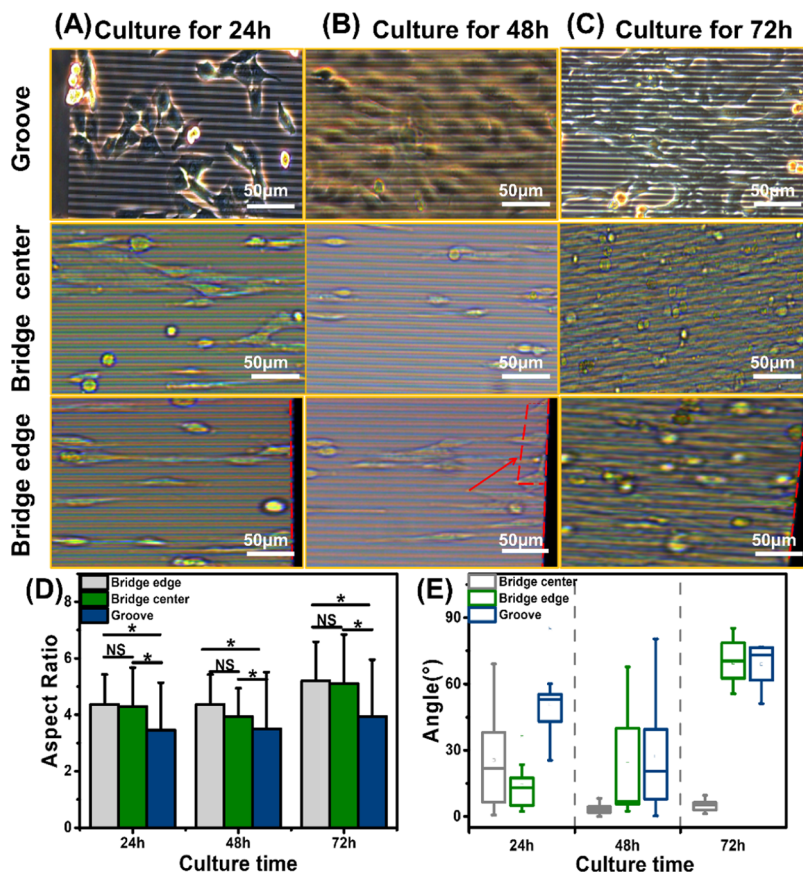

Figure 3. (A–C) Phase contrast images of cells located on microgrooved substrates (depth = 2 μm) and boundary, the center of microbridges, at different culture times. (D) Aspect ratio of cells located on microbridge boundary, microbridge center, and microgrooves ($n = 50$). (E) Alignment analysis of cells located on the microbridge boundary, microbridge center, and microgrooves at cultures of 24, 48, and 72h ($n = 50$).

The surface morphologies of the microgrooves and microbridges were characterized by scanning electron microscopy (SEM). The microgrooves and suspended microbridge structure were successfully fabricated using this method as
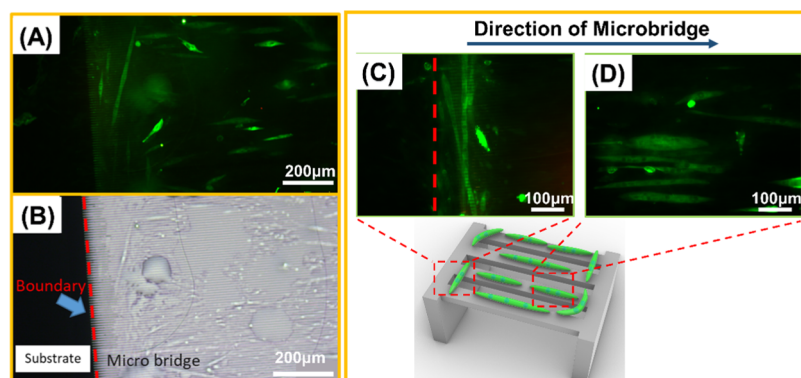
Figure 4. (A) Cells seeded on microbridge substrates were differentiated and then stained for the myosin heavy chain (MHC). White scale bars equal 100 μm. (B) Phase contrast image of the myotubes on microbridges. White scale bars equal 100 μm. (C, D) Myotubes located on different regions of microbridged substrates show different orientations.

shown in Figure 1E,F. Then, myoblasts were seeded on substrates to explore the influence of topology on cell behavior (Figure 1G,H).

3.2. Effects of Substrate Depth on Myoblast Behaviors.

To distinguish the effects of substrate depths on myoblast behaviors, microgrooved substrates (width of 5 μm) with touchable depth (0.5, 2 μm) and microgrooves (width of 5 μm) with untouchable depth were fabricated, and the bare glass substrate was kept as the control group (Figure 2A−D). Subsequently, C2C12 myoblasts were seeded on substrates with different depths, and the cell morphologies were quantitatively analyzed. The spreading area of the cells cultured on bare glass, the microgrooved substrates with a depth of 0.5 and 2 μm, and microbridges were 1339.96 $\pm$ 465.76, 835.28 $\pm$ 216.90, 759.65 $\pm$ 221.16, and 593.26 $\pm$ 167.22 μm^2 respectively (Figure 2E). The cell aspect ratios increased from 3.71 $\pm$ 1.36 to 4.68 $\pm$ 1.29 with the increase in substrate depth (Figure 2F). Quantification of the spreading area and the aspect ratios of cells on the substrate with various depths revealed that the increase of substrate depth inhibited cell spreading but promoted cell elongation.

The directional distribution of myotubes on microgrooved substrates is depicted in Figure 2G. Myoblasts cultured on the bare glass displayed a relatively randomized alignment, while myoblasts cultured on microgrooved substrates with depths of 0.5 and 2 μm showed a bias-angular cell orientation. The proportion of cells oriented along within $\pm$10° increased with increasing depth (from 6% for the control group to 30% for the group with a depth of 2 μm), indicating that the orientation along the microgrooves becomes pronounced with increasing depth. However, about 92% of the cells at microbridges showed a significant orientation along topological features. The more concentrated angular distribution of myoblasts with increasing depth revealed the promotional effects of the microgroove depth on cell alignment (Figure 2H).

3.3. Cell Behavior on the Anisotropic Substrate at Different Times.

Images of cells located on microgrooves and microbridges were taken at 24, 48, and 72 h of culture, respectively (Figure 3A−C). Cell elongation is critical for myoblast fusion and further influences the contraction of myotubes. To quantify cell elongation on different substrates, aspect ratios were measured (Figure 3D). With increasing culture time, the aspect ratios of the cells on microgrooves with a depth of 2 μm (from 3.15 $\pm$ 1.14 for 24 h to 3.82 $\pm$ 0.84 for 72 h) and microbridges (from 4.02 $\pm$ 1.29 for 24 h to 4.67 $\pm$ 1.29 for

72 h) were increased, indicating that the increase of the culture time promoted the elongation of cells on the substrate. Besides, the aspect ratios of the cells on the microbridge substrate were always greater than those on microgroove substrates. These results indicated that the microbridge structure with an untouchable depth had more obvious promotional effects on cell elongation.

Cell alignment plays a pivotal role in tissue engineering for blood vessels, neural nets, and especially skeletal muscle. There are various factors that affect cell alignment and ultimately the function of engineered tissues. As shown in Figure 3A, myoblasts elongated on the microgrooved substrates and showed a uniform orientation at 24 h. The statistical results of cell alignment angles showed that the cells cultured on the microgrooved substrates showed a bias-angular (50.82 $\pm$ 16.14°) cell orientation (Figure 3E). With the prolonged culture time, cells located on microgrooved substrates maintained their bias-angular orientation. Besides, the angular distribution of cells on microgrooves becomes more concentrated, which implied the promotional effects of microgrooves on cell alignment guidance.

Besides, the cells cultured on microbridges displayed an orientation (14.16 $\pm$ 10.46°) along microbridges at 24 h of culture (Figure 3E). Interestingly, cells located on the microbridge edge tend to change their orientation with the prolonged culture time and displayed a position-dependent orientation. The cell alignment angle on the center of microbridge substrates decreased from 25.55 $\pm$ 21.83 to 5.08 $\pm$ 2.71° for 72 h, which showed a more pronounced orientation along microbridges with increasing culture time. Nevertheless, the alignment angle of the cells cultured on the edges of the microbridges increased from 14.16 $\pm$ 10.46 to 69.73 $\pm$ 10.34°. The increasing alignment angle revealed the transition of cell orientation from parallel to perpendicular to the microbridge. The above-mentioned results indicated that the orientation of the cells was closely related to the topological structure of the substrates.

3.4. Differentiation Results of C2C12 Myoblasts on Microbridges.

To determine the influence of substrate depth on myoblast differentiation, C2C12 myoblasts were differentiated into myotubes by differentiation medium supplemented with 2% horse serum after 72 h of culture. C2C12 myoblasts grew on the silicon nitride microbridge substrates and differentiated into myotubes. Subsequently, the differentiated myotubes were stained with a myosin heavy chain to obtain clear
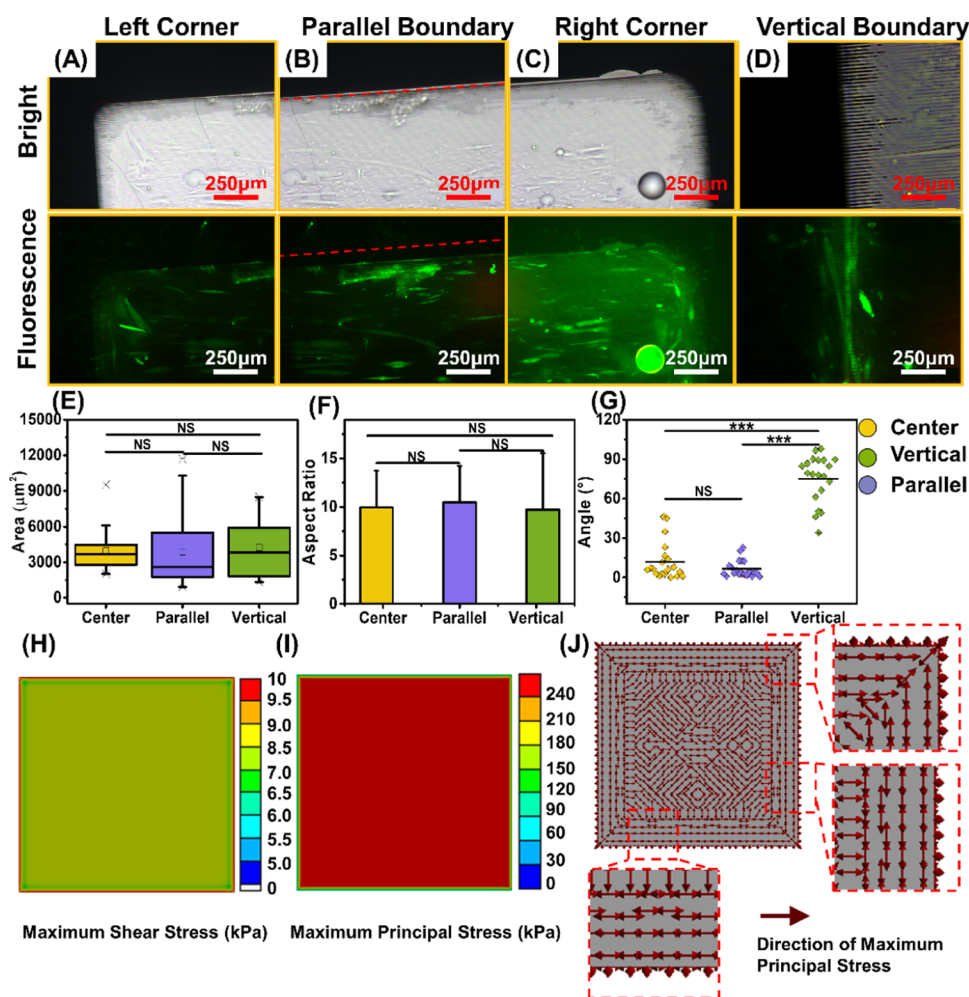
Figure 5. (A−D) Phase contrast images and fluorescence images of myotubes located on the left corner, parallel boundary, right corner, and vertical boundary of microbridge substrates. (E−G) Area, aspect ratio, and orientation of myotubes located on the center (yellow), parallel boundary (purple), and vertical (green) of microbridge substrates ($n = 30$). (H−J) Predictions of the in-plane maximum shear stress, value, and direction of maximum principal stresses in the cell layer.

cell images (Figure 4A,B). As demonstrated in Figure 4C,D, myotubes displayed quite different orientations in different regions of microbridge substrates. This position-dependent orientation was mainly manifested in that the myotubes in the middle of the microbridge were mainly oriented along the direction of the microbridge, while the orientation of the myotube in other regions was related to the location of the region. At the boundary perpendicular to the microbridge structure, the myotube was mainly oriented along the direction perpendicular to the microbridge structure. The myotube was mainly oriented along the direction of the microbridge substrates at the boundary parallel to the microbridge structure.

Cell orientation is critical to the function and structural integrity of engineered tissues; therefore, it is necessary to quantify the cell orientation on the microbridge substrates. Since the myotubes had different orientations in different regions of the microbridge, the regions of microbridge substrates can be categorized into left corner, right corner, parallel boundary, and vertical boundary (Figure 5A−D). The left corner and right corner correspond to the left or corner of microbridge substrates; the parallel boundary and vertical boundary correspond to the boundary of microbridge substrates that are parallel or perpendicular to microbridges. The immunofluorescence images of myotubes in different regions of the

microbridge substrates implied that myotubes displayed an orientation depending on the location (Figure 5A−D). Myotubes at the left and right corners of the microbridge substrate tended to bend and grow along the direction of the corner (Figure 5A). As depicted in Figure 5C, the myotubes located at a parallel boundary showed a significant orientation along the microbridges. Nevertheless, the myotubes at the vertical boundary displayed an orientation perpendicular to the microbridge (Figure 5D) orientations.

Myotubes are formed by the fusion of multiple myoblasts, and their area and aspect ratio are usually positively correlated to the number of myoblasts fused. As a consequence of myoblast fusion, the area and aspect ratio of myotubes are increased with an increasing number of fused cells, which suggests a potential capacity for greater force output. Besides, myotubes always contract along the long axis of myotubes in response to electrical stimulation. Hence, the orientation of the myotube is another factor that affects its function. To characterize the morphology of myotubes, we measured their area, aspect ratio, and orientation angle. There was no significant difference in the area of the myotubes at the center ($3945.28 \pm 1747.09 \ \mu m^2$), vertical boundary ($3860.11 \pm 3071.68 \ \mu m^2$), and parallel boundary ($4223.43 \pm 2560.72 \ \mu m^2$) of the microbridges (Figure 5E). The aspect ratios of the myotubes on the center, parallel

boundary, and vertical boundary of microbridge substrates were 9.84 ± 3.89, 8.83 ± 1.83, and 10.36 ± 3.47, respectively (Figure 5F). Quantification results of the area and aspect ratio indicated that the locations of myotubes did not affect the differentiation degree of myotubes.

Subsequently, the myotube orientation was quantified by measuring the alignment angle of myotubes. The alignment angle is defined as the angle between the long axis of myotubes and the main axis of microbridges. As shown in Figure 5G, the alignment angles of myotubes located in the center, parallel boundary, and vertical boundary of microbridge substrates were 5.61 ± 3.31, 4.4 ± 3.08, and $82.52 \pm 7.89°$, respectively. This implied that the orientation of the myotubes was strongly related to the region of the myotubes.

To further analyze the reasons for the position-dependent orientation of C2C12 myoblasts on the microbridges, the shear and principal stress of cell layers with corners were simulated by thermal contraction (Figure 5H−J). We found that the shear and principal stress at the edge of the structure were larger than in other regions. Cells are usually oriented along the direction of maximum principal stress.[39,40] The results of the principal stress direction showed that there was a clear position-dependent maximum principal stress distribution at the edges and corners, which was consistent with the experimental results of cell orientation. These results implied that the edge constraints affected the stress field and polarization direction of the cell layer, suggesting that the myoblast orientation on the microbridges was a unique biomechanical behavior guided by the topology.

4. DISCUSSION

Our results indicated that the anisotropic topological cues influence myoblast growth, elongation, and alignment due to contact guidance. Quantitative results of the cell aspect ratio indicated that the depth of substrates plays a key role in cell elongation. This promotional effect of cell aspect ratio became more dominant with increasing depth and culture time but was irrelevant to the cell location. As the depth of the substrate increased, the alignment angle decreased, which implied that the orientation of the cells along the microgrooves becomes more obvious (Figure 6A). Nevertheless, cells on microbridges with

Figure 6. Depth sensing of myoblasts during myogenic differentiation. (A) Response of myoblasts to the depth of anisotropic structures. (B) Myogenic differentiation maintains the depth response of myoblasts.

untouchable depth displayed a position-dependent orientation that aligned along microbridges at the center region and parallel boundary but perpendicular to the microbridge on the vertical boundary.

Mechanical interactions between cells and topological cues are essential for cellular sensing and alignment. Cells are equipped with several different mechanisms to sense the physical characteristics of the microenvironment and the mechanical forces generated therein. Among the numerous components of cells, filopodia play a key role in exploring the microenvironment, generating mechanical forces, and performing chemical signaling for cell topological response. Therefore, we hypothesize that cells will reach the bottom and sidewall of the microgrooves by extending the filamentous pseudopodia as cells cultured on anisotropic substrates. Then, myoblasts form an anchor point and bend the cytoskeleton, which causes the cells to cross the groove and result in chiral deflection. Thus, the C2C12 cells can sense and respond to the topological structure of substrates and show a bias-angular orientation relative to the microgrooves (Figure 6A). Nevertheless, as the depth increases, the formation of the anchor point at the substrate requires a greater degree of cytoskeleton bending and energy expenditure. Hence, the myoblasts show a more pronounced tendency to align along the anisotropic structure with increasing depth.

When the depth of anisotropic structures increases to an untouchable depth, the bending of the cytoskeleton cannot reach the bottom of the substrate to form an anchor point, so the cells cannot cross the adjacent microgrooves. The center region of the microbridges can be considered the microgrooves with untouchable depth, so the cells in the central region and parallel boundaries of the microbridges are always oriented along the microbridges. As for the vertical edge of the microbridge, they form a continuous domain, and the existence of the edge makes the direction of the maximum principal stress of cells change from along the microbridge to perpendicular to the microbridge (Figure 5J). Thus, cells on the vertical edge can form vertical cell bridges under the guidance of the vertical continuous domain through the migration of the population of cells. In response to topologies, C2C12 myoblasts display different orientations at the early stage of culture, which further affects their fusion and function (Figure 6B). Moreover, the morphology of myotubes on microgrooves maintained the bias-angular orientation, and myotubes on microbridges exhibit distinct position-dependent orientations. The design of tissue engineering scaffolds could aid in ensuring the customization of the muscle tissue structure and function.

5. CONCLUSIONS

In conclusion, we have demonstrated that cells displayed different elongation and alignment behaviors in response to the topology and depth of substrates. The decrease in the cell spreading area with increasing depth indicated that increasing depth leads to the limitation of cell spreading. Moreover, the elongation of C2C12 myoblasts along the topological structure direction was promoted with the increase in substrate depth. Thus, myoblasts on the microgrooved substrates showed a more concentrated orientation aligned (from 6 to 30% of cells) to microgrooves with increasing depth. To further investigate the influence of depth, microbridged substrates with untouchable depth were fabricated. Cells cultured on microbridges had a larger aspect ratio that was irrelevant to the cell location on the microbridge, which also confirmed the promotional effect of the substrate depth on the cell elongation. The cell morphology
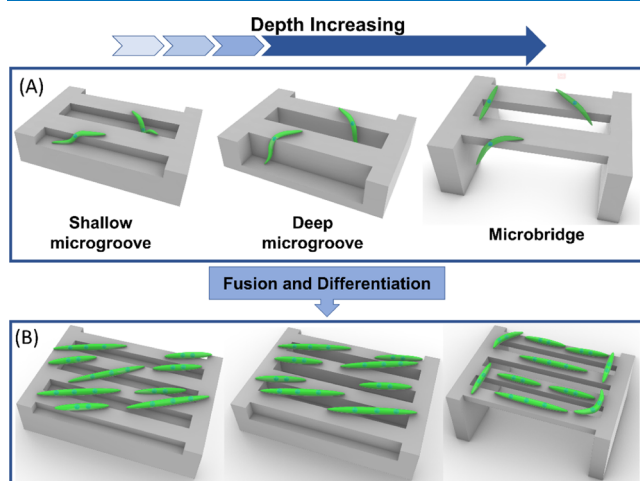
determination implied that the cells displayed various behaviors in different regions of the microbridge substrates. Briefly, cells in the center region and the parallel boundary of substrates were oriented along the microbridge, while cells on the vertical edge were oriented perpendicular to the microbridge. The differentiated myotubes maintained the orientation of the myoblasts, which showed a position-dependent orientation. The analysis of the cell layer stress implied that the position-dependent orientation of cells on the microbridge substrate is closely related to the depth sensing of cells due to substrate discontinuity. This work reveals the underlying mechanism of myoblast depth sensing and contact guidance behaviors, contributing to engineered skeletal muscle patterning, which suggests a potential application in biohybrid actuation.

■ AUTHOR INFORMATION

Corresponding Author

Xiaoxiao Chen − *School of Advanced Manufacturing, Nanchang University, Nanchang 330031 Jiangxi, P. R. China;* ⦿ orcid.org/0000-0001-5497-8600; Email: chenxx@ncu.edu.cn

Authors

Jianfeng Chen − *School of Advanced Manufacturing, Nanchang University, Nanchang 330031 Jiangxi, P. R. China;* ⦿ orcid.org/0000-0002-9248-4844

Xuefei Chen − *School of Advanced Manufacturing, Nanchang University, Nanchang 330031 Jiangxi, P. R. China*

Yihao Ma − *School of Advanced Manufacturing, Nanchang University, Nanchang 330031 Jiangxi, P. R. China*

Yiran Liu − *School of Advanced Manufacturing, Nanchang University, Nanchang 330031 Jiangxi, P. R. China*

Jin Li − *School of Advanced Manufacturing, Nanchang University, Nanchang 330031 Jiangxi, P. R. China*

Kai Peng − *School of Advanced Manufacturing, Nanchang University, Nanchang 330031 Jiangxi, P. R. China*

Yichuan Dai − *School of Advanced Manufacturing, Nanchang University, Nanchang 330031 Jiangxi, P. R. China*

Complete contact information is available at:
https://pubs.acs.org/10.1021/acsomega.3c04981

Author Contributions

J.C., X.C., and Y.M. contributed to the conception and design of the study. Y.L. and J.L. performed the experiments and analyzed the data. Y.M. and K.P. contributed to writing—review and editing. X.C. and Y.D. contributed to original draft writing. J.C. contributed to funding acquisition and review. All authors contributed to article revision and read and approved the submitted version. All authors reviewed this article, contributed, and approved the final article.

Funding

Notes

The authors declare no competing financial interest.

■ ACKNOWLEDGMENTS

■ REFERENCES

(1) Ma, Y.; Han, T.; Yang, Q.; et al. Viscoelastic Cell Microenvironment: Hydrogel-Based Strategy for Recapitulating Dynamic ECM Mechanics. *Adv. Funct. Mater.* **2021**, *31* (24), No. 2100848.

(2) Dunn, A.; Talovic, M.; Patel, K.; et al. Biomaterial and stem cell-based strategies for skeletal muscle regeneration. *J. Orthop. Res.* **2019**, *37* (6), 1246−1262.

(3) Xu, Y.; Zhou, J.; Liu, C.; et al. Understanding the role of tissue-specific decellularized spinal cord matrix hydrogel for neural stem/progenitor cell microenvironment reconstruction and spinal cord injury. *Biomaterials* **2021**, *268*, No. 120596.

(4) Vernerey, F. J.; Sridhar, S. L.; Muralidharan, A.; et al. Mechanics of 3D Cell-Hydrogel Interactions: Experiments, Models, and Mechanisms. *Chem. Rev.* **2021**, *121* (18), 11085−11148.

(5) Rizwan, M.; Tse, J. W.; Nori, A.et al. Cell−Substrate Interactions. In *Principles of Regenerative Medicine*; Elsevier, 2019; Chapter 27, pp 437−468.

(6) Zhang, K.; Xiao, X.; Wang, X.; et al. Topographical patterning: characteristics of current processing techniques, controllable effects on material properties and co-cultured cell fate, updated applications in tissue engineering, and improvement strategies. *J. Mater. Chem. B* **2019**, *7* (45), 7090−7109.

(7) Yang, Y.; Wang, K.; Gu, X.; et al. Biophysical Regulation of Cell Behavior-Cross Talk between Substrate Stiffness and Nanotopography. *Engineering* **2017**, *3* (1), 36−54.

(8) Coyle, S.; Doss, B.; Huo, Y.; et al. Cell alignment modulated by surface nano-topography - Roles of cell-matrix and cell-cell interactions. *Acta Biomater.* **2022**, *142*, 142149−142159.

(9) Pan, Y.; Jiang, D.; Gu, C.; et al. 3D microgroove electrical impedance sensing to examine 3D cell cultures for antineoplastic drug assessment. *Microsyst. Nanoeng.* **2020**, *6*, No. 23.

(10) Zhang, W.; Yang, Y.; Cui, B.; et al. New perspectives on the roles of nanoscale surface topography in modulating intracellular signaling. *Curr. Opin Solid State Mater. Sci.* **2021**, *25* (1), No. 100873, DOI: 10.1016/j.cossms.2020.100873.

(11) Nouri-Goushki, M.; Isaakidou, A.; Eijkel, B. I. M.; et al. 3D printed submicron patterns orchestrate the response of macrophages. *Nanoscale* **2021**, *13* (34), 14304−14315.

(12) Chaudhuri, P. K.; Wang, M. S.; Black, C. T.; et al. Modulating T Cell Activation Using Depth Sensing Topographic Cues. *Adv. Biosyst.* **2020**, *4* (9), No. e2000143.

(13) Oyunbaatar, N. E.; Shanmugasundaram, A.; Lee, D. W.; et al. Contractile behaviors of cardiac muscle cells on mushroom-shaped micropillar arrays. *Colloids Surf., B* **2019**, *174*, 174103−174109.

(14) Pan, Z.; Yan, C.; Peng, R.; et al. Control of cell nucleus shapes via micropillar patterns. *Biomaterials* **2012**, *33* (6), 1730−1735.

(15) Liu, X.; Liu, R.; Cao, B.; et al. Subcellular cell geometry on micropillars regulates stem cell differentiation. *Biomaterials* **2016**, *111*, 11127−11139.

(16) Wilson, R. E.; Denisin, A. K.; Dunn, A. R.; et al. 3D Microwell Platforms for Control of Single Cell 3D Geometry and Intracellular Organization. *Cell. Mol. Bioeng.* **2021**, *14* (1), 1−14.

(17) Jin, Y.; Shahriari, D.; Jeon, E. J.; et al. Functional Skeletal Muscle Regeneration with Thermally Drawn Porous Fibers and Reprogrammed Muscle Progenitors for Volumetric Muscle Injury. *Adv. Mater.* **2021**, *33* (14), No. e2007946.

(18) Chen, X.; Du, W.; Cai, Z.; et al. Uniaxial Stretching of Cell-Laden Microfibers for Promoting C2C12 Myoblasts Alignment and Myofibers Formation. *ACS Appl. Mater. Interfaces* **2020**, *12* (2), 2162−2170.

(19) Zhao, M.; Liu, H.; Zhang, X.; et al. A flexible microfluidic strategy to generate grooved microfibers for guiding cell alignment. *Biomater. Sci.* **2021**, *9* (14), 4880−4890.

(20) Thrivikraman, G.; Jagiełło, A.; Lai, V. K.; et al. Cell contact guidance via sensing anisotropy of network mechanical resistance. *Proc. Natl. Acad. Sci. U.S.A.* **2021**, *118* (29), No. e2024942118, DOI: 10.1073/pnas.2024942118.

(21) Patel, K. H.; Talovic, M.; Dunn, A. J.; et al. Aligned nanofibers of decellularized muscle extracellular matrix for volumetric muscle loss. *J. Biomed. Mater. Res., Part B* **2020**, *108* (6), 2528−2537.

(22) Gao, H.; Xiao, J.; Wei, Y.; et al. Regulation of Myogenic Differentiation by Topologically Microgrooved Surfaces for Skeletal Muscle Tissue Engineering. *ACS Omega* **2021**, *6* (32), 20931−20940.

(23) Ray, A.; Lee, O.; Win, Z.; et al. Anisotropic forces from spatially constrained focal adhesions mediate contact guidance directed cell migration. *Nat. Commun.* **2017**, *8*, No. 14923.

(24) Lu, K.; Qian, Y.; Gong, J.; et al. Biofabrication of aligned structures that guide cell orientation and applications in tissue engineering. *Bio-Des. Manuf.* **2021**, *4* (2), 258−277.

(25) Leclech, C.; Barakat, A. I. Is there a universal mechanism of cell alignment in response to substrate topography? *Cytoskeleton* **2021**, *78* (6), 284−292.

(26) Leclech, C.; Villard, C. Cellular and Subcellular Contact Guidance on Microfabricated Substrates. *Front. Bioeng. Biotechnol.* **2020**, *8*, No. 551505.

(27) Chen, X.; Xia, Y.; Du, W.; et al. Contact Guidance Drives Upward Cellular Migration at the Mesoscopic Scale. *Cell. Mol. Bioeng.* **2023**, *16* (3), 205−218.

(28) Zhang, D.; Suo, H.; Qian, J.; et al. Physical understanding of axonal growth patterns on grooved substrates: groove ridge crossing versus longitudinal alignment. *Bio-Des. Manuf.* **2020**, *3* (4), 348−360.

(29) Zhang, Q.; Li, Y.; Sun, H.; et al. hMSCs bridging across micro-patterned grooves. *RSC Adv.* **2015**, *5* (59), 47975−47982.

(30) Tabdanov, E. D.; Puram, V.; Zhovmer, A.; et al. Microtubule-Actomyosin Mechanical Cooperation during Contact Guidance Sensing. *Cell Rep* **2018**, *25* (2), 328−338.e5.

(31) Song, L.; Wang, K.; Li, Y.; et al. Nanotopography promoted neuronal differentiation of human induced pluripotent stem cells. *Colloids Surf., B* **2016**, *148*, 14849−14858.

(32) Buskermolen, A. B. C.; Suresh, H.; Shishvan, S. S.; et al. Entropic Forces Drive Cellular Contact Guidance. *Biophys. J.* **2019**, *116* (10), 1994−2008.

(33) Li, M.; Fu, X.; Gao, H.; et al. Regulation of an osteon-like concentric microgrooved surface on osteogenesis and osteoclasto-genesis. *Biomaterials* **2019**, *216*, No. 119269.

(34) Fraser, S. A.; Ting, Y.; Mallon, K. S.; et al. Sub-micron and nanoscale feature depth modulates alignment of stromal fibroblasts and corneal epithelial cells in serum-rich and serum-free media. *J. Biomed. Mater. Res., Part A* **2008**, *86A* (3), 725−735.

(35) Chua, J. S.; Chng, C. P.; Moe, A. A. K.; et al. Extending neurites sense the depth of the underlying topography during neuronal differentiation and contact guidance. *Biomaterials* **2014**, *35* (27), 7750−7761.

(36) Lee, K.; Kim, E. H.; Oh, N.; et al. Contribution of actin filaments and microtubules to cell elongation and alignment depends on the grating depth of microgratings. *J. Nanobiotechnol.* **2016**, *14* (1), No. 35.

(37) Huang, J.; Chen, Y.; Tang, C.; et al. The relationship between substrate topography and stem cell differentiation in the musculoske-letal system. *Cell. Mol. Life Sci.* **2019**, *76* (3), 505−521.

(38) Chen, J.; Zhong, M. Fabrication and release of silicon nitride micro string array by convection freeze sublimation method at atmospheric pressure. *J. Micromech. Microeng.* **2018**, *28* (10), No. 105019, DOI: 10.1088/1361-6439/aad603.

(39) He, S.; Green, Y.; Saeidi, N.; et al. A theoretical model of collective cell polarization and alignment. *J. Mech. Phys. Solids* **2020**, *137*, No. 103860.

(40) He, S.; Liu, C.; Li, X.; et al. Dissecting Collective Cell Behavior in Polarization and Alignment on Micropatterned Substrates. *Biophys. J.* **2015**, *109* (3), 489−500.